JACS
JOURNAL OF THE AMERICAN CHEMICAL SOCIETY
Article
pubs.acs.org/JACS

Predicted Lithium–Boron Compounds under High Pressure

Feng Peng,[†,‡] Maosheng Miao,[§] Hui Wang,[†] Quan Li,[†] and Yanming Ma*[,†]

[†]State Key Laboratory of Superhard Materials, Jilin University, Changchun 130012, People's Republic of China
[‡]College of Physics and Electronic Information, Luoyang Normal University, Luoyang 471022, People's Republic of China
[§]Materials Department and Materials Research Laboratory, University of California, Santa Barbara, California 93106-5050, United States

Supporting Information

ABSTRACT: High pressure can fundamentally alter the bonding patterns of light elements and their compounds, leading to the unexpected formation of materials with unusual chemical and physical properties. Using an unbiased structure search method based on particle-swarm optimization algorithms in combination with density functional theory calculations, we investigate the phase stabilities and structural changes of various Li–B systems on the Li-rich regime under high pressures. We identify the formation of four stoichiometric lithium borides (Li_3B_2, Li_2B, Li_4B, and Li_6B) having unforeseen structural features that might be experimentally synthesizable over a wide range of pressures. Strikingly, it is found that the B–B bonding patterns of these lithium borides evolve from graphite-like sheets in turn to zigzag chains, dimers, and eventually isolated B ions with increasing Li content. These intriguing B–B bonding features are chemically rationalized by the elevated B anionic charges as a result of Li→B charge transfer.

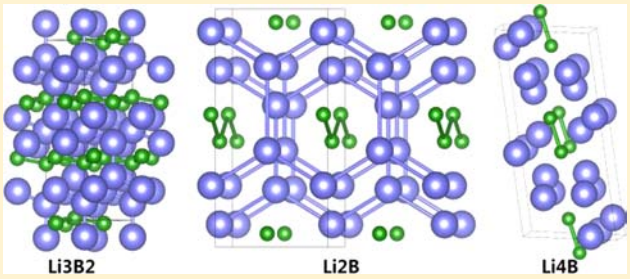

INTRODUCTION

Light elements (e.g., Li, B, and C) and their compounds often present extraordinary chemical bonding features, especially at extreme conditions, that can give lead to novel physical properties, such as superconductivity, metal–insulator transitions, and superhardness.[1−6] Because of the short bond lengths, the 2p orbitals of C can form π bonds, leading to the formation of graphene sheets, polymer chains, and dimers.[7,8] Recently, a graphene-like B sheet in MgB_2 has attracted intensive interest because of the unexpected transition to a high superconducting state at 39 K.[9] The stabilization of this B sheet might be intimately related to the fact that B^- ions are isoelectronic to C atoms. Other B structures that are analogous to C, such as polymer chains, have not been perceived. Perhaps these structures may also form if more electrons are transferred to B.

Chemically, the mixing of Li and B in the Li-rich regime can produce Li–B compounds with B ions in a high anionic charge state; therefore, they are ideal systems for exploring the evolution of B–B bonding features with increasing charge states of B. Unfortunately, the Li–B systems in the Li-rich regime are not stable at ambient conditions, except for $LiB_{0.88}$, in which B atoms form a carbyne-like chain intercalated in a hexagonal close-packed (hcp) Li lattice.[10] It is known that high pressure can stabilize the chemical systems which are unstable at ambient conditions.[11] It is therefore essential to investigate the phase stabilities and fundamental structures of Li–B systems in the Li-rich regime under high pressures in order to probe B–B bonding patterns with the variation of charge states of B.

Although the search for Li–B compounds under ambient and high pressures has been of constant interest over the past four decades,[10,12−19] only a few such compounds, including Li_3B_{14}, Li_2B_6, and $LiB_{0.88}$, have been reliably characterized.[10,12,13] The ion and electron conductivity of these compounds[20] and their possible application as intercalation electrodes[21] have been investigated. These compounds are primarily on the B-rich side of the Li–B binaries and are electron poor. Their structures feature complicated polyhedral B networks with Li sitting in the interstitial sites in order to overcome the electron deficiency of B.

In contrast to the B-rich systems, there is little work on the Li-rich borides, from both the experimental and theoretical sides. In this composition regime, B exists in higher anionic charge states and can possess unique bonding features, analogous to C. In this work, we systematically investigated the phase stabilities of stoichiometric Li_xB (x = 1, 1.5, 2, 2.5, 3–8) compounds under various pressures ranging from 0 to 200 GPa, and identified their structures and bonding patterns. We utilized a combination of an unbiased structural search based on a particle-swarm optimization (PSO) algorithm[22] and a first-principles density functional total energy calculation to explore the entire configuration space. The effectiveness of our method has been demonstrated by recent successes in predicting high-pressure structures of various systems, ranging from elements to binary and ternary compounds.[23]

Received: August 27, 2012
Published: October 22, 2012

ACS Publications © 2012 American Chemical Society

dx.doi.org/10.1021/ja308490a | J. Am. Chem. Soc. 2012, 134, 18599–18605

METHODS

We performed structure predictions through a global minimization of free energy surfaces based on the CALYPSO (Crystal structure AnaLYsis by Particle Swarm Optimization) methodology as implemented in CALYPSO code.[22] We searched the structures of stoichiometric Li_xB (x = 1, 1.5, 2, 2.5, 3−8) with simulation cell sizes of 1−4 formula units (f.u.) in a pressure range from 0 to 200 GPa. The local structural relaxations and electronic band structure calculations were performed in the framework of density functional theory within the generalized gradient approximation and frozen-core all-electron projector-augmented wave (PAW) method,[24] as implemented in the VASP code.[25] The adopted PAW pseudopotentials of Li and B treat 1s, 2s, and 2p electrons as valence. The cutoff energy of 700 eV and appropriate Monkhorst−Pack[26] k-meshes were chosen to ensure that all the enthalpy calculations were well converged to less than 1 meV/atom. The phonon calculations were carried out by using a finite displacement approach[27] through the PHONOPY code.[28]

RESULTS AND DISCUSSION

1. Phase Diagram. We first investigated the phase stabilities of Li−B systems in Li-rich stoichiometry by calculating the formation enthalpy of various Li_xB compounds in a pressure range of 0 to 200 GPa. The formation enthalpy of Li_xB was calculated by using fractional representation Li_yB_{1-y} ($0 < y < 1$) with respect to the decomposition into LiB and Li, as

$$h^f(Li_yB_{1-y}) = h(Li_yB_{1-y}) - (1-y)h(LiB) - (2y-1)h(Li) \quad (1)$$

where the enthalpies h for Li_yB_{1-y} and LiB are obtained for the most stable structures as searched by the CALYPSO method at the desired pressures. For Li, the known structures of bcc, fcc, hR9, cI16, oC40, oC24, and oC56[29] are considered in their corresponding stable pressure ranges. The convex hulls are depicted in Figure 1 for pressures of 0, 50, 100, and 200 GPa. A particular Li−B compound was defined to be "stable" only if its enthalpy of formation was the lowest, while a defined "metastable" system was one which is found on the convex hull; i.e., its h^f was lower than the sum of h^f values of the two decomposition products. Notably, the stable or metastable systems, as defined above, might be experimentally synthesizable. The validity of using LiB instead of B in defining h^f is ensured by the fact that LiB is exceedingly stable with respect to other Li−B systems above 40 GPa, as revealed by our study (see below) and another recent work,[30] and consideration of the more stable nonstoichiometry $LiB_{0.88}$ below 40 GPa will not modify the convexity.

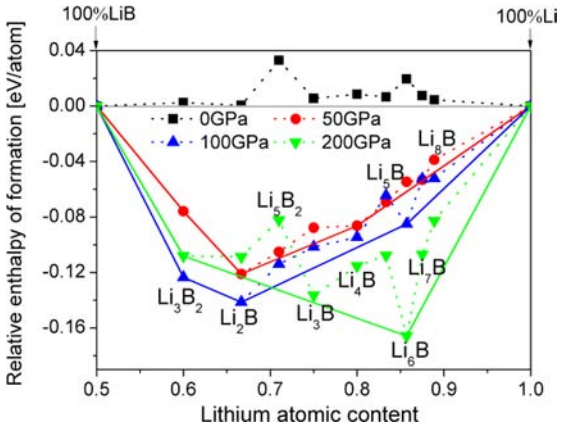

Figure 1. Relative enthalpies of formation per atom with respect to LiB and Li for different Li−B phases. The convex hulls are shown by solid lines. Dotted lines through the neighboring points residing above the convex hull are guides for the eye.

Our main results can be summarized as follows: (i) At P = 0 GPa, all the Li_xB ($x > 1$) systems which have positive h^f are not stable. This is consistent with the experimental observation that no Li_xB compound or alloy forms at ambient pressure. (ii) At P = 50 GPa, the h^f values of all stoichiometries are negative. Among different compositions, Li_2B is the most stable stoichiometry; Li_3B_2, Li_2B, and Li_4B are metastable systems. (iii) At P = 100 GPa, Li_2B remains as the most stable composition, while Li_3B_2, Li_2B, and Li_6B are metastable. (iv) At P = 200 GPa, the most stable composition turns out to be Li_6B, and Li_3B_2 is the only metastable system.

The shift of the phase stability toward Li-rich compositions with increasing pressure is accompanied by a series of structural changes promoted by variations in B−B bonding patterns. With an increase in Li content, the bonding features of B evolve from graphene-like sheets (LiB and Li_3B_2 phases) in turn to one-dimensional chains (Li_2B and Li_5B_2 phases), a mixture of one-dimensional chains and B_2-dimers (Li_3B phase), B_2-dimers (Li_4B phase), and eventually isolated B atoms enclosed by Li cages (Li_xB phases, $x \geq 5$).

The strong association of the B bonding feature with the Li content originates from the charge state of the B atoms. Figure 2 shows the anionic and cationic charges of B and Li atoms in the series of Li−B compounds at 100 GPa calculated by the Bader analysis.[31] For Li_xB ($x \leq 5$) systems, the Li charges are almost constant, and the B charges increase almost linearly with the Li content. For Li_xB ($x > 5$), the B charges become saturated at a value of 3.5, whereas the Li charges decrease with increasing Li content. Our calculations reveal a strong correlation between the B coordination and its anionic charge state. The underlying reason for how the charge states alter the bonding feature will be analyzed later. Although the charge transfers are not integer and are smaller than the formal charges of Li and B, the Li_xB ($x \leq 5$) systems can be considered as

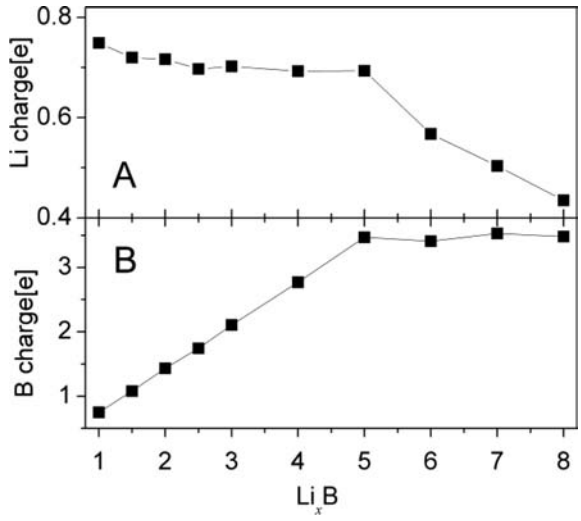

Figure 2. Calculated cationic and anionic charges of Li (A) and B (B) ions in different Li_xB systems. The predicted most stable structures for different Li_xB compositions in the context are used for the Bader charge calculations. Structures of Li_5B, Li_7B, and Li_8B are depicted in the Supporting Information.

dx.doi.org/10.1021/ja308490a | J. Am. Chem. Soc. 2012, 134, 18599−18605

nearly completely ionic. The noninteger charges are due to the fact that the charges are calculated by partitioning space according to its zero-flux surfaces. As a matter of fact, using the Bader charge analysis, we find that the Na charge in a typical ionic crystal NaCl is around 0.83.

It is important to recognize that, in light-element systems (elements and their compounds), ion dynamics can significantly change the total energies originating from the large zero-point energy (ZPE) contribution. As a result, the ZPEs for the *Cmcm* structure of Li_2B, the NaTl structure of LiB, and the oC40 structure of Li at 100 GPa are calculated to be as large as 129, 145, and 94 meV/atom, respectively. However, the contribution of ZPE to h^f is typically small. In the case of Li_2B, it is only about 1 meV/atom. Therefore, it is valid to neglect the contribution of ZPE when discussing the relative stability of Li–B systems.

2. LiB. The structure of LiB at ambient pressure has been intensively studied experimentally in the past decade. An unexpected incommensurate structure was found, in which Li atoms form a hexagonal close-packed sublattice interpenetrated by hexagonally arrayed one-dimensional chains of B atoms. Not only is the B sublattice incommensurate to the Li sublattice, but also the B atoms along the chains are disordered.[10] As a result, LiB is a nonstoichiometric system at ambient pressure. It has been shown both experimentally and theoretically that LiB_x has a wide range of stable forms ($0.82 < x < 1.0$) with almost no energy barrier between the different phases, even at zero temperature.[11] At pressures >30 GPa, this incommensurate feature disappears and the most stable phase adopts stoichiometry LiB, as revealed by a systematic calculation of $Li_{2n}B_m$ ($2n > m$) by Kolmogorov et al.[11]

We searched for structures of LiB with simulation cell sizes of 1–8 f.u., in a pressure range from 0 to 500 GPa. Our results show that $P6_3/mmc$ (Figure 3A, Table S1) is the most stable structure at ambient conditions (Figure S1), in good agreement with the results of Kolmogorov et al.[11] and Rosner et al.[32] The $P6_3/mmc$ structure transforms to $R\bar{3}m$ phase (Figure 3D, Table S2) at 1 GPa and then to a layered $P6_3/mmc$ phase (Figure 3C, Table S3) at 42 GPa. Under pressures >70 GPa, the NaTl structure (Figure 3B, Table S4) becomes most stable. All four structures are demonstrated to be dynamically stable in their respective pressure ranges by phonon calculations (Figures S2–S5).

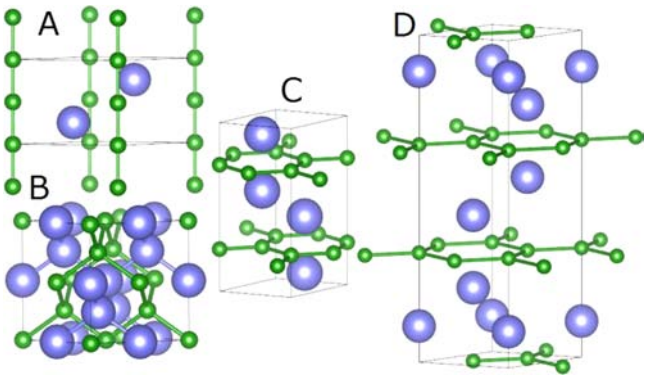

Figure 3. Predicted structures of LiB at ambient and high pressures. The green and purple balls represent B and Li atoms, respectively. (A) $P6_3/mmc$ structure. (B) NaTl ($Fd\bar{3}m$) structure. (C) Layered $P6_3/mmc$ structure. (D) $R\bar{3}m$ structure. Structural details are given in the Supporting Information.

Using Bader charge analysis, we found that one valence electron of Li is almost completely transferred to B, leading to the 1− charged B in LiB, which is isoelectronic to C. Therefore, the B lattices in the LiB structures are chemically comparable to the allotropes of C. The B chain in $P6_3/mmc$ structure is thus analogous to a carbyne chain[7,8] in which a C atom is in sp hybridization. Similar to carbyne chains, the sp orbitals in B^- chains form σ bonds between neighboring B atoms, and the $2p_y$ and $2p_z$ orbitals form π bonds. The electron localization function (ELF; see Figure S6) sheds light on the bonding character. A B^- chain would be metallic because the bands are half filled. This is confirmed by our electronic structure calculations, showing that the $P6_3/mmc$ phase is metallic and the electronic states around the Fermi level consist mainly of B p orbitals (Figure S7). A major difference between C and B^- is that the latter has a smaller nuclear charge; therefore, the radius of its orbitals is larger. This is consistent with the fact that the C–C bond lengths are shorter than the analogous B^-–B^- distances (Table 1).

Table 1. Structural Data on B–B, Li–Li, and Li–B Bond Lengths [Å] and Formal Electron Count per B Atom as Well as the Density of States (DOS) at the Fermi Level [states/eV, f.u.], Which Directly Affects the Conductivity Properties for Various Li–B Systems at Certain Pressures [GPa]

	LiB	Li_3B_2	Li_2B	Li_4B	Li_6B
pressure [GPa]	0	100	100	50	100
B–B	1.56	1.75	1.64	1.63	3.58
Li–Li	2.79	1.85	1.83	1.89	1.59
Li–B	2.44	1.85	1.92	2.06	2.18
formal electron count	1	1.5	2	4	5
DOS at Fermi level (E_f)	0.34	0.47	0.48	0.94	0.51

In the intermediate pressure range, the structures consisting of graphite-like B^- layers (layered $P6_3/mmc$ and $R\bar{3}m$) are stabilized. The layers are buckled, similar to the B^- layer in MgB_2. As in a graphite layer, the sp^2-hybridized orbitals form a network of σ bonds, and the other two p orbitals form delocalized π bonds. Therefore, the LiB phases in $P6_3/mmc$ and $R\bar{3}m$ structures are also metallic, as shown by their calculated DOS (Figure S8). The σ and π bonding feature can also be seen from our calculated ELF (Figures S9 and S10).

At a pressure higher than 70 GPa, LiB is stabilized in the NaTl structure, in which the B^- ions and Li^+ ions form two interpenetrating diamond lattices. The B covalent network is again analogous to C structures, wherein diamond is stabilized over graphite at a pressure around 1.4 GPa.[33] Compared to diamond, the sp^3-hybridized orbitals of B^- form a three-dimensional σ bond network (Figure S11). Because of the splitting of the bonding and the antibonding states, the B^- lattice and therefore the whole LiB compound should be insulating or semiconducting. This is confirmed by the calculated band structure and the DOS (Figure S12). The band gap of the NaTl structure has an intriguing pressure dependence (Figure S13), showing a direct→indirect bandgap transformation. After a thorough structure search, we concluded that LiB is stable in the NaTl structure up to 500 GPa.

3. Li_3B_2. From the convex hull (Figure 1), Li_3B_2 is stable at 50, 100, and 200 GPa. By structure searching at 50, 100, and 200 GPa, we find a unique hexagonal structure with $R\bar{3}m$ symmetry (Table S6, space group 166) to be the most stable.

dx.doi.org/10.1021/ja308490a | J. Am. Chem. Soc. 2012, 134, 18599–18605

That is to say, Li_3B_2 has no phase transition in a pressure range of 50−200 GPa. This structure is demonstrated to be dynamically stable in its stable pressure ranges by phonon calculations (Figure S17). Similar to the $R\bar{3}m$ and the layered $P6_3/mmc$ structures for LiB, the B atoms in Li_3B_2 also form graphite-like sheets, separated by Li ions, and buckle (similar to a B monolayer[34]) under pressure. Their major difference is the stacking since Li_3B_2 has more Li atoms. As shown in Figure 4A, the stacking sequence is (LiBLi)Li(LiBLi)Li... .

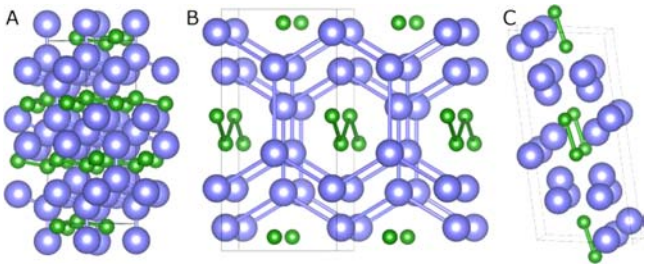

Figure 4. Predicted structures of (A) Li_3B_2, (B) Li_2B, and (C) Li_4B at 50 GPa. The green and purple balls represent B and Li atoms, respectively.

Similar to LiB, the B atoms are in sp^2 hybridization and are connected by the σ bonds formed between the sp^2 orbitals of neighboring B atoms. This character can be seen from the calculated ELF (Figure S18). The $2p_z$ orbital electrons form the π bond. Unlike LiB, there is an extra electron transferred from Li to each B atom; therefore, the π bands should be completely filled. However, the band structure and the DOS show that Li_3B_2 is metallic (Figure 5). By looking into the *l*- and *m*-resolved projected density of states (PDOS), we find that the metallicity originated from incomplete filling of the σ bands.

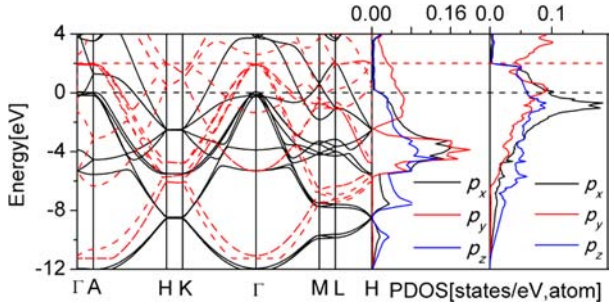

Figure 5. Electronic band structure and PDOS for Li_3B_2 at 100 GPa. In the left panel, the black solid lines are the electronic band structure of Li_3B_2; the red dashed lines are those of $Li_0B_2^{3-}$ in which all the Li atoms are removed from the Li_3B_2 structure. The black and red dashed lines show the Fermi energy of Li_3B_2 and $Li_0B_2^{3-}$, respectively. The middle and right panels present the DOS of Li_3B_2 and $Li_0B_2^{3-}$ projected on the three p orbitals.

We constructed a model system, $Li_0B_2^{3-}$, in which all the Li ions are removed from the $R\bar{3}m$ structure. Three extra electrons and a uniform compensated background charge were added so that the system was isoelectronic to Li_3B_2. The bands were aligned by the electrostatic potential at the PAW core radius. As shown in Figure 5, the shapes of the bands match well for the two systems, but there is a large energy shift. Compared with $Li_0B_2^{3-}$, the Li^+ ions in Li_3B_2 can greatly lower the energy of the π bands, resulting in a $\pi \rightarrow \sigma$ charge transfer that drives the hole doping of the σ bands. This feature is similar to LiB[11] and MgB_2,[35] which is a major factor that causes the superconductivity in these two compounds.

4. Li_2B. The convex hull (Figure 1) shows that Li_2B is the most stable at 50 and 100 GPa. Li_2B is predicted to adopt the *Cmcm* structure (Figure 4B, Table S7) throughout its stable pressure range (50−100 GPa). In this structure, the B atoms form kinked chains along the *c* axis, and each chain is surrounded by a hexagonal Li tube. The B−B bond length within the B chains is 1.64 Å (Table 1) at 100 GPa.

In order to investigate the physical mechanism behind the chemical reactions LiB + Li → Li_2B at high pressures, we plot out the volume of Li_2B together with the total volume of LiB + Li as a function of pressure, as shown in Figure 6A. It is seen

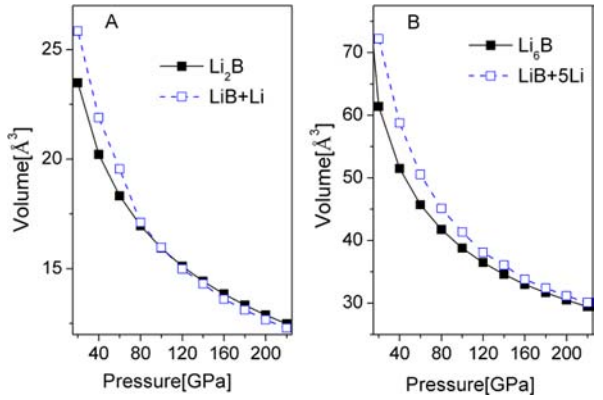

Figure 6. Pressure dependence of the volumes (per f.u.) of (A) Li_2B and LiB + Li and (B) Li_6B and LiB + 5Li.

that the total volume of LiB + Li is evidently larger than that of Li_2B at pressures <104 GPa. This volume reduction is a driving force for the formation of Li_2B. At higher pressures, the total volume of LiB + Li becomes smaller than that of Li_2B, promoting the decomposition of Li_2B into LiB and Li. This might also be the underlying origin for the instability of Li_2B at 200 GPa, as indicated by the convex hull (Figure 1).

Through the Bader charge analysis, it is found that there is almost complete charge transfer from Li to B atoms. As a result, each B atom possesses five valence electrons and is in a 2− charge state which is isoelectronic to C^-. While negative C ions are important in organic molecules, it is interesting to study the bonding behavior of B^{2-} in solid states.

In order to further characterize the charge transfer and the bonding features, we calculated the ELF of four systems: Li_2B, hypothetical Li_0B (all Li atoms removed), Li_0B^{2-}, and hypothetical Li_2B_0 (all B atoms removed) (Figure 7). As shown in Figure 7A, the ELF of Li_2B suggests that no covalent bonds exist between Li and B, indicating a strong ionic feature of the compound. Figure 7D shows that Li atoms have a strong tendency to contribute their electrons to B atoms at high pressures. Even if the B atoms are removed from the structure, large amounts of charges are transferred to the interstitial regions. The ELF of Li_2B (Figure 7A) also shows strong covalent bonds between B ions. It is noteworthy that the B−B bond length within the B chains is 1.65 Å, which is larger than the bond length of a double B═B bond (1.59 Å; see Table 1) and smaller than that of a single B−B bond (1.78 Å).[10] We also find that the B−B−B angles are 124°, indicating that the B orbitals are in sp^2 hybridization. The zigzag chains are interconnected by the σ bonds between the sp^2 orbitals located

dx.doi.org/10.1021/ja308490a | J. Am. Chem. Soc. 2012, 134, 18599−18605

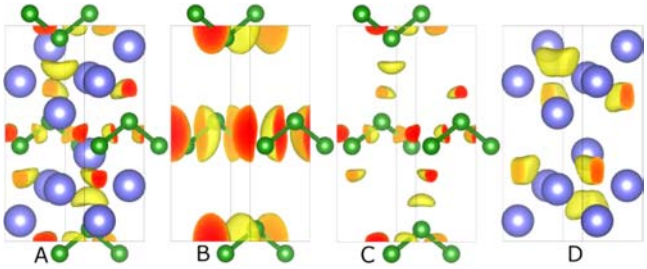

Figure 7. Calculated ELF of (A) Li_2B, (B) a hypothetical bare orthorhombic structure of Li_0B (all Li atoms removed from Li_2B), (C) Li_0B^{2-}, and (D) a hypothetical Li_2B_0 (all B atoms removed from Li_2B) at 100 GPa. The green and the purple balls represent B and Li atoms, respectively. The isosurface value is set as 0.85.

at the neighboring B ions, and the $2p_z$ orbital electrons form the π bond. The major difference between the B^{2-}–B^{2-} chains in Li_2B and the B^-–B^- chains in LiB is the existence of a lone pair of electrons in B^{2-} ions which occupy one sp^2 orbital. Because of the delocalization of the π electrons, Li_2B should also be metallic, as supported by the calculated band structure and the DOS (Figure S20).

Another possible way of bonding B^{2-} is to have the lone pairs occupy the $2p_z$ orbitals and the sp^2 orbitals form a layered σ bond network. This arrangement is high in energy due to the stronger Coulomb repulsions between the $2p_z$ lone pairs at the neighboring B ions. Therefore, no structures featuring a B^{2-} sheet were ever found by our structure searches.

In order to reveal the effect of the charge redistribution, the ELFs of hypothetical bare orthorhombic structures of Li_0B (Li atoms removed) and Li_0B^{2-} (with two negative charges and Li atoms removed) are examined in Figure 7B,C. The ELF of Li_0B (Figure 7B) shows no σ bonds and lone pairs formed by the sp^2 orbitals on B, whereas these features are clearly seen in the ELF of the Li_0B^{2-} system (Figure 7C). This bonding feature of B^{2-} also illustrates its effect on the band structure. The bands of Li_2B, Li_0B^-, and Li_0B^{2-} around the Fermi level are all contributed by the B s and p orbitals. The situation can be generally described by a rigid band model; namely, the change in the electron filling of the bands has little effect on the dispersion of the bands. This is consistent with the fact that the band structure of Li_0B^- (Figure S21A) around the Fermi level is very different from that of Li_2B, whereas the band structure of Li_0B^{2-} (Figure S21B) is very similar to that of Li_2B since the electron filling is the same for the two systems.

5. Li_4B. As shown in Figure 4C, the predicted structure of Li_4B is monoclinic $C2/m$ (Table S11). In this structure, the B ions form B–B dimers. This is because B^{4-} ions have seven electrons and need to form three lone pairs. Only one electron can be involved in forming a single σ bond with a neighboring B^{4-} ion, causing the formation of B–B dimers with a B–B bond length of 1.83 Å (Table 1) at 50 GPa. This distance is very similar to the B–B bond length (1.82 Å) of B–B dimers in V_3B_2 at ambient pressure.[36]

6. Li_6B. Li_6B is an exciting example of Li–B compounds in the Li-rich side. The number of Li atoms exceeds the highest formal valence of 5− for B (Figure 2). As a result, the system is remarkably electron rich. The convex hull (Figure 1) shows that Li_6B is the most stable at 200 GPa. After thorough structure searches, we find that Li_6B crystallizes in a fascinating hexagonal $R\bar{3}m$ structure (Figure 8A, Table S17) that is stable above 100 GPa. This structure can be viewed as an assembly of

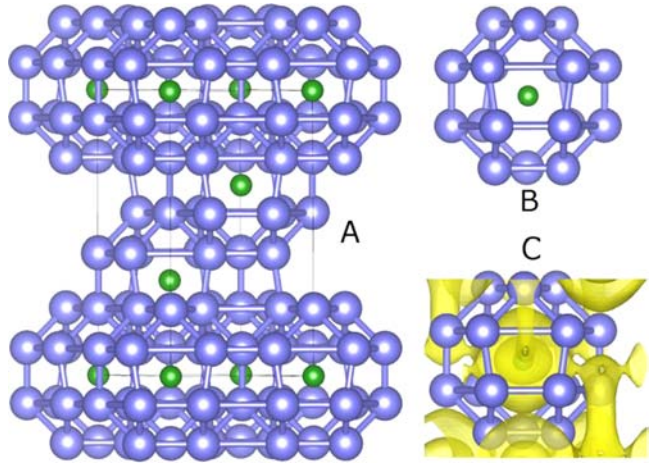

Figure 8. (A) Predicted structure of Li_6B at 100 GPa. The green and the purple balls represent B and Li atoms, respectively. (B) An isolated B ion and the surrounding icosahedral cage of Li. (C) Calculated ELF within one $Li_{18}B$ unit. The isosurface value is set as 0.73.

$Li_{18}B$ units (Figure 8B), where the B atoms form a hR1 lattice (the high-pressure phase of elemental Li[37]) and are enclosed by an icosahedron of Li. In a icosahedral $Li_{18}B$ unit, the nearest Li–B interatomic distances are nearly equal (the difference is only 0.005 Å). That is to say, every B atom has 18 near-neighboring Li atoms, and each Li atom has 3 near-neighboring B atoms. Therefore, the stoichiometry is Li_6B. A $Li_{18}B$ unit is composed of 8 triangles and 12 quadrilaterals. Li atoms can be classified into four different layers: the top and bottom layers are forming triangle Li_3 rings, while the middle two layers consist of hexagonal Li_6 rings.

Here, the formation of Li_6B is intimately related to the volume reduction due to a higher packing efficiency in Li_6B. As shown in Figure 6B, the volume of one Li_6B unit is significantly smaller than the total volume of LiB + 5Li in a large pressure range.

A partial charge transfer from Li was clearly shown by the Bader analysis as depicted in Figure 2. A comparison of the band structures of Li_6B, Li_6B_0 (all B atoms removed from Li_6B), and Li_0B (all Li atoms removed from Li_6B) offered further support. Even without the presence of B, the valence bandwidth of the hypothetical Li_6B_0 (Figure 9B) is already 3.2 eV, comparable to 2.8 eV for Li_6B (Figure 9A). The valence bandwidth of the Li_0B (B in hcp lattice) is only 0.8 eV (Figure 9C). The electronic band dispersions of Li_6B from −2.8 to 1.5 eV were remarkably similar to those of Li_6 from −1.1 to 2.5 eV. The band structure of Li_6B near the Fermi level was modified from Li_6 due to the mixing between B 2p and Li 2s or 2p orbitals (from PDOS of Figure 9A).

The dense packing of Li_6B originates from the high ionic states of the atoms. There are six Li atoms per unit. In principle, six electrons of Li are transferable to B. In reality, however, B accepts a maximum of five of them, forming a charge state of 5− (Figure 2), and its 2p states are completely filled. This prevents the formation of any B–B bonds; therefore, B in Li_6B adopts an intriguing state of isolated ions. On the other hand, the high ionic charge of B causes much stronger electrostatic interactions with the surrounding Li ions, leading to shorter Li–B distances. As a matter of fact, the Li–B distance in Li_6B is 2.02 Å at 200 GPa, significantly smaller than that of 2.40 Å in LiB. Because of the closer Li–B distances, the Li–Li distances

dx.doi.org/10.1021/ja308490a | J. Am. Chem. Soc. 2012, 134, 18599–18605

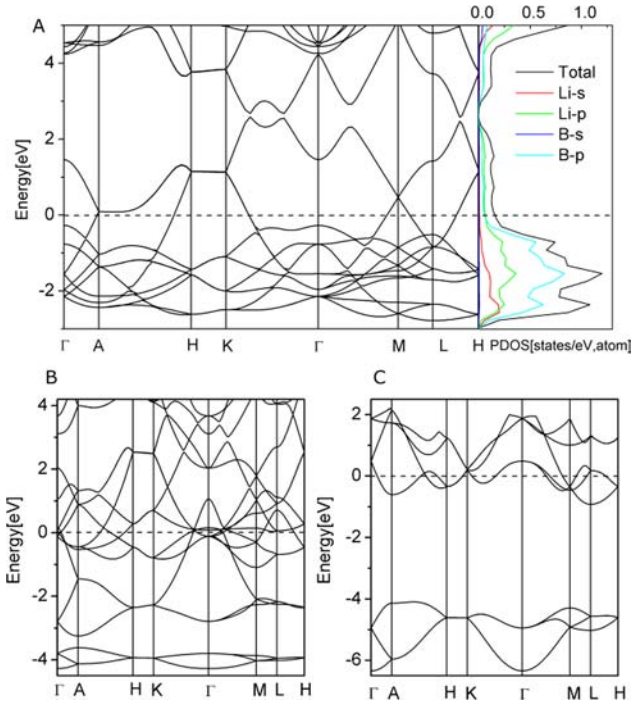

Figure 9. (A) Electronic band structure (left) and PDOS (right) of Li_6B at 200 GPa. (B) Band structure of Li_6B_0. (C) Band structure of Li_0B.

are also very small. At 200 GPa, it is 1.59 Å, close to the radius of the Li 2s orbital.

The exceedingly dense packing of Li_6B gives rise to many interesting bonding features. As shown by the band structure and the PDOS in Figure 9, Li_6B is metallic. The states around the Fermi level consist mainly of Li 2s and 2p states. It was found recently that elemental Li undergoes a structural transition under a pressure of 60 or 70 GPa[23c,29c] and becomes a semiconductor. The underlying mechanism is the complete localization of valence electrons at the interstitial region in a densely packed Li lattice. In contrast, Li_6B remains metallic at pressures as high as 200 GPa. The ELF (Figure 8C) shows a large electron density variation in the interstitial region; however, it is not strong enough to cause the metal−insulator transition as in pure Li.

CONCLUSION

Using a structure search method based on CALYPSO methodology and density functional total energy calculations, we systematically studied the phase stabilities and the structures of Li−B systems in the Li-rich regime. We identify four novel stoichiometric Li_xB compounds with unexpected structures that might be experimentally synthesizable over a wide range of pressures, including Li_3B_2, Li_2B, Li_4B, and Li_6B. Our results reveal a general trend in the structural changes featuring different B lattices with increasing Li content, namely from a graphite-like B sheet in Li_3B_2 to zigzag B chains in Li_2B, to B dimers in Li_4B, and finally to isolated B ions in Li_6B. By analyzing the electronic structure and the electron localization functions, we reveal that the above trend is caused by the increasing anionic charge of B. As the anionic charge increases, the B ions acquire more and more lone pair electrons that are not involved in forming chemical bonds with the neighboring B ions, leading to a lower coordination number, and eventually to an isolated B surrounded by an icosahedral Li cluster.

ASSOCIATED CONTENT

Supporting Information

Computational details, crystal structure information, electronic properties, phonon dispersion curves, band structures, electronic DOS, and ELF curves for various stoichiometry under different pressures. This material is available free of charge via the Internet at http://pubs.acs.org.

AUTHOR INFORMATION

Corresponding Author

mym@jlu.edu.cn or mym@calypso.cn

Notes

The authors declare no competing financial interest.

ACKNOWLEDGMENTS

We are highly grateful to Prof. Roald Hoffmann and Dr. Andreas Hermann for their constructive comments on our manuscript and the exchange of information on their unpublished results on various Li−B phases. This work is supported by the China 973 Program (2011CB808200), Natural Science Foundation of China under 11274136, 11104104, 11025418 and 91022029, the 2012 Changjiang Scholars Program of China, Changjiang Scholar and Innovative Research Team in University (IRT1132), and the research fund of Key Laboratory of Surface Physics and Chemistry (SPC201103). M.M. thanks the ConvEne-IGERT Program (NSF-DGE0801627) and the MRSEC program (NSF-DMR1121053).

REFERENCES

(1) Zhou, R.; Zeng, X. C. *J. Am. Chem. Soc.* **2012**, *134*, 7530−7538.
(2) Xue, M.; Chen, G.; Yang, H.; Zhu, Y.; Wang, D.; He, J.; Cao, T. *J. Am. Chem. Soc.* **2012**, *134*, 6536−6539.
(3) Matsuoka, T.; Shimizu, K. *Nature* **2009**, *458*, 186−189.
(4) Hermann, A.; Ivanov, B. L.; Ashcroft, N. W.; Hoffmann, R. *Phys. Rev. B* **2012**, *86*, 014104.
(5) Li, Q.; Ma, Y.; Oganov, A. R.; Wang, H.; Xu, Y.; Cui, T.; Mao, H.; Zou, G. *Phys. Rev. Lett.* **2009**, *102*, 175506.
(6) Braun, C.; Börger, S. L.; Boyko, T. D.; Miehe, G.; Ehrenberg, H.; Höhn, P.; Moewes, A.; Schnick, W. *J. Am. Chem. Soc.* **2011**, *133*, 4307−4315.
(7) Rice, M. J.; Bishop, A. R.; Campbell, D. K. *Phys. Rev. Lett.* **1983**, *51*, 2136.
(8) Hoffmann, R.; Janiak, C.; Kollmar, C. *Macromolecules* **1991**, *24*, 3725−3746.
(9) Nagamatsu, J.; Nakagawa, N.; Muranaka, T.; Zenitani, Y.; Akimitsu, J. *Nature* **2001**, *410*, 63−64.
(10) (a) Wörle, M.; Nesper, R. *Angew. Chem.* **2000**, *112*, 2439−2443. (b) Wörle, M.; Nesper, R. *Angew. Chem., Int. Ed.* **2000**, *39*, 2349−2353. (c) Wörle, M.; Nesper, R.; Chatterji, T. K. *Z. Anorg. Allg. Chem.* **2006**, *632*, 1737−1742. (d) Lazicki, A.; Hemley, R. J.; Pickett, W. E.; Yoo, C. *Phys. Rev. B* **2010**, *82*, 180102.
(11) (a) Kolmogorov, A. N.; Curtarolo, S. *Phys. Rev. B* **2006**, *73*, 180501. (b) Kolmogorov, A. N.; Curtarolo, S. *Phys. Rev. B* **2006**, *74*, 224507. (c) Kolmogorov, A. N.; Calandra, M.; Curtarolo, S. *Phys. Rev. B* **2008**, *78*, 094520.
(12) Mair, G.; Nesper, R.; Schnering, H. G. v. *J. Solid State Chem.* **1988**, *75*, 30−40.
(13) Mair, G.; Schnering, H. G. v.; Wörle, M.; Nesper, R. *Z. Anorg. Allg. Chem.* **1999**, *625*, 1207−1211.
(14) Secrist, R. D. *J. Am. Chem. Soc.* **1967**, *50*, 520−523.

(15) Sorokin, V. P.; Gavrilov, P. I.; Levakov, E. V. *Russ. J. Inorg. Chem.* **1977**, *22*, 329−330.
(16) James, S. D.; DeVries, L. E. *J. Electrochem. Soc.* **1976**, *123*, 321−327.
(17) (a) Wang, F. E.; Mitchell, M. A.; Sutula, R. A.; Holden, J. R.; Bennett, L. H. *J. Less-Common Met.* **1978**, *61*, 237−251. (b) Mitchell, M. A.; Sutula, R. A. *J. Less-Common Met.* **1978**, *57*, 161−175.
(18) Serebryakova, I. I.; Lyashenko, V. I.; Levandovskii, V. D. *Powder Metallurgy Met. Ceram.* **1994**, *33*, 49.
(19) Meden, A.; Mavri, J.; Bele, M.; Pejovnik, S. *J. Phys. Chem.* **1995**, *99*, 4252−4260.
(20) (a) Gunji, S.; Kamimura, H.; Nakayama, T. *J. Phys. Soc. Jpn.* **1993**, *62*, 2408−2418. (b) Matsuda, H.; Nakayama, T.; Kimura, K.; Murakami, Y.; Suematsu, H.; Kobayashi, M.; Higashi, I. *Phys. Rev. B* **2004**, *52*, 224505.
(21) Dallek, S.; Ernst, D. W.; Larrick, B. F. *J. Electrochem. Soc.* **1979**, *126*, 866−870.
(22) (a) Wang, Y.; Lv, J.; Zhu, L.; Ma, Y. *Phys. Rev. B* **2010**, *82*, 094116. (b) Wang, Y.; Lv, J.; Zhu, L.; Ma, Y. *Comput. Phys. Commun.* **2012**, *183*, 2063−2070. (c) CALYPSO code is free for academic use, please register at http://www.calypso.cn.
(23) (a) Wang, H.; Tse, J. S.; Tanaka, K.; Iitaka, T.; Ma, Y. *Proc. Natl. Acad. Sci. U.S.A.* **2012**, *109*, 6463−6466. (b) Zhu, L.; Wang, Z.; Wang, Y.; Zou, G.; Mao, H.; Ma, Y. *Proc. Natl. Acad. Sci. U.S.A.* **2012**, *109*, 751−753. (c) Wang, Y.; Liu, H.; Lv, J.; Zhu, L.; Wang, H.; Ma, Y. *Nature Commun.* **2011**, *2*, 563. (d) Lv, J.; Wang, Y.; Zhu, L.; Ma, Y. *Phys. Rev. Lett.* **2011**, *106*, 015503. (e) Zhu, L.; Wang, H.; Wang, Y.; Lv, J.; Ma, Y.; Cui, Q.; Ma, Y.; Zou, G. *Phys. Rev. Lett.* **2011**, *106*, 145501. (f) Nishio-Hamane, D.; Zhang, M.; Yagi, T.; Ma, Y. *Am. Mineral.* **2012**, *97*, 568−572.
(24) (a) Blöchl, P. E. *Phys. Rev. B* **1994**, *50*, 17953−17979. (b) Kresse, G.; Joubert, D. *Phys. Rev. B* **1999**, *59*, 1758−1775.
(25) Kresse, G.; Furthmüller, J. *Phys. Rev. B* **1996**, *54*, 11169.
(26) Monkhorst, H. J.; Pack, J. D. *Phys. Rev. B* **1976**, *13*, 5188.
(27) Parlinski, K.; Li, Z. Q.; Kawazoe, Y. *Phys. Rev. Lett.* **1997**, *78*, 4063.
(28) Togo, A.; Oba, F.; Tanaka, I. *Phys. Rev. B* **2008**, *78*, 134106.
(29) (a) Overhauser, A. W. *Phys. Rev. Lett.* **1984**, *53*, 64. (b) Hanfland, M.; Syassen, K.; Christensen, N. E.; Novikovet, D. L. *Nature* **2000**, *408*, 174−178. (c) Matsuoka, T.; Shimizu, K. *Nature* **2009**, *458*, 186−189. (d) Ma, Y.; Oganov, A. R.; Xie, Y. *Phys. Rev. B* **2008**, *78*, 014102. (e) Deemyad, S.; Schilling, J. *Phys. Rev. Lett.* **2003**, *91*, 167001.
(30) (a) Hermann, A.; Suarez-Alcubilla, A.; G. Gurtubay, I.; Yang, L.; Bergara, A.; Ashcroft, N. W.; Hoffmann, R. *Phys. Rev. B* **2012**, *86*, 144110. (b) Hermann, A.; McSorley, A.; Ashcroft, N. W.; Hoffmann, R. *J. Am. Chem. Soc.* **2012**, DOI: 10.1020/ja308492g.
(31) Tang, W.; Sanville, E.; Henkelman, G. *J. Phys.: Condens. Matter* **2009**, *21*, 084204.
(32) Rosner, H.; Pickett, W. *Phys. Rev. B* **2003**, *67*, 054104.
(33) Bundy, F. P.; Bovenkerk, H. P.; Strong, H. M.; Wentorf, R. H. J. *Chem. Phys.* **1961**, *35*, 383−391.
(34) Wu, X.; Dai, J.; Zhao, Y.; Zhuo, Z.; Yang, J.; Zeng, X. C. *ACS Nano* **2012**, *6*, 7443−7453.
(35) An, J. M.; Pickett, W. E. *Phys. Rev. Lett.* **2001**, *86*, 4366.
(36) Riabov, A. B.; Yartys, V. A.; Hauback, B. C.; Guegan, P. W.; Wiesinger, G.; Harris, I. R. *J. Alloys Compd.* **1999**, *293*−*295*, 93−100.
(37) (a) Hanfland, M.; Syassen, K.; Christensen, N. E.; Novikov, D. L. *Nature* **2000**, *408*, 174−178. (b) Guillaume, C.; Gregoryanz, E.; Degtyareva, O.; McMahon, M.; Hanfland, M.; Evans, S.; Guthrie, M.; Sinogeikin, S.; Mao, H. *Nat. Phys.* **2011**, *7*, 211−214.